Experimental Thermal and Fluid Science 151 (2024) 111074

Contents lists available at ScienceDirect

Experimental Thermal and Fluid Science

journal homepage: www.elsevier.com/locate/etfs

Apparatus and methods for the calibration and correction of a polydispersed dust feeding system applied in multiphase flow experiments

Alessio Suman *, Nicola Zanini, Alessandro Vulpio, Michele Pinelli

Department of Engineering, University of Ferrara, Via Giuseppe Saragat 1, 44121, Italy

ARTICLE INFO

Keywords:
Aerosol
Calibration
Isokinetic sampling
Spectrometer
Multiphase experiments

ABSTRACT

Multiphase flow experiments allow the understanding of complex interaction mechanisms between particles and fluid structures under controlled conditions. In standard test rigs, the airflow is mixed with precise dust amount continuously, and accurate knowledge of the aerosol amount injected is mandatory to achieve reliable measurements and results. This work proposes the experimental procedure for calibrating an aerosol dosing and injection system. The purpose-built calibration system layout is explained in detail. To give a general perspective of the procedure, four test powders commonly used in multiphase flow tests have been used: Alumina, Silicon Carbide, and two grades of standard soil named Arizona Road Dust. Methodologies and criticisms are reviewed and assessed, and the final results are given in the form of calibration curves of the feeding system. Since the proposed correction is based on powder and flow characteristics, the proposed methodology can be applied to several cases and conditions.

1. Introduction

Aerosol measurements in flowing air are typically conducted in wind tunnel facilities. The design process of wind tunnels is strictly related to the purpose of the study and the phenomena under investigation. The guidelines for wind tunnel design provided by Rae and Pope [1] in the 1980s are still used nowadays. The critical aspect is controlling the flow field to generate stable and repeatable measurement conditions. Wind tunnels are classified by the velocity range achieved in the test section: low speed (Mach number less than 0.4) and high speed (Mach number over 0.4). Similar facilities were used in multiphase flow experiments with the key difference related to the aim of the investigation. Low-speed wind tunnels have been typically used in aerosol measurements to investigate aerosol sampling techniques. These rigs, characterized by a low velocity of the air (from 0.5 m/s to 4 m/s), are used to develop and validate sampling theories [2] or to test sampling instruments and techniques [3 –6]. For example, Belyaev and Levin [3] investigated the influence of the sampling probe aspiration coefficient on concentration estimation. Similar studies have been provided by Witschger et al. [7], which investigated the sampling efficiency of a wind tunnel facility.

Furthermore, low-speed wind tunnels have also been realized in aerosol science to understand fundamental mechanisms such as deposition and resuspension of micrometric particles. Wind tunnels have been used to investigate phenomena related to the interaction of the particles with flow structures or wall surfaces. In most cases, the particle-to-surface interaction can be detrimental to the long-term life of the components. The interaction of particles with solid surfaces may lead to deposition [8 –10] or erosion issues [11,12]. In operative conditions, particle deposition and erosion phenomena lead to recoverable and unrecoverable performance deterioration of devices and systems [13 –15]. Due to the variety of the operative conditions of such devices, the test facilities used to replicate these phenomena have different configurations. The interaction between substrate and particles involves several aspects related to particle characteristics and flow field phenomena, which can be controlled only using wind tunnel facilities [16 –19].

Particle-wall interaction is significant in the case of turbomachinery and heat exchanger, which operates with contaminated airflow or gases. Looking at turbomachinery, particles dispersed in the flow can cause erosion or deposition on compressor blades [16,20] and turbine components [21,22]. These phenomena are responsible for the deterioration of the engine over time [23]. For this reason, several test rigs have been realized to investigate the blade surface deterioration due to erosion [24] and deposition [21,25]. In those facilities, particles are injected and accelerated up to 200 m/s to reproduce the flow field inside a real engine. Heat exchangers are also affected by particle deposition issues. In those devices, the deposit build-up on surfaces causes the reduction of

* Corresponding author.
E-mail address: alessio.suman@unife.it (A. Suman).

https://doi.org/10.1016/j.expthermflusci.2023.111074
Received 7 August 2023; Received in revised form 23 September 2023; Accepted 10 October 2023
Available online 13 October 2023

Nomenclature

C	concentration
$\widehat{C}$	actual concentration
$\overline{C}$	measured concentration
C_D	drag coefficient
d	particle diameter
e	mass error
F_D	drag force
i	diameter beam index
k	total number of beam
L	reference length
M	mass (referred to a particle)
m	mass flow rate
N	particle number distribution
Re	Reynold number
Stk	Stokes number
U	flow velocity
ρ	density
μ	viscosity

Acronyms

AoR	angle of repose
ARD	arizona road dust
N	nominal
RS	ring speed
UF	ultra fine

Subscript and superscript

0	referred to undisturbed flow
air	referred to the air
p	referred to particle
mean	referred to the mean particle
0.3	ring thickness of 0.3 mm
1.0	ring thickness of 1.0 mm
10	referred to the 10 % of particles
50	referred to the 50 % of particles
90	referred to the 90 % of particles

the heat transfer over time. Experimental investigations and theoretical models on this topic have been provided through field inspections [26]. Furthermore, experimental test facilities have been realized to offer systematic studies of the fouling of heat exchangers [14,27 –30].

1.1. Dosing and dispensing systems

Such applications are characterized by the interaction of contaminated airflow (an airflow stream carries solid particles) and components (blades, fins, etc.) under different airflow velocities, temperature values, and humidity conditions. Beyond the complexity of such a system, the experimental analysis has to control the contamination of the airflow precisely to ensure a proper correlation between the actual operating condition and the experimental results [17,18]. To control the airflow contamination, the system has to be equipped with a feeder and dosing systems able to store, prepare, and provide the contaminants (i.e., solid particles) during the tests. In particular, the metering and dispensing of solid particles change according to application and the solid particle characteristics [31]. According to the [32], feeder technology can be divided depending on the operating pressure, i.e., low pressure (up to 1 bar), medium-pressure (up to 3 bar) and high-pressure systems (up to 10 bar). The proper system selection should be based on particle characteristics (particle size, cohesive, friable, free flowing, whether degradation or high temperature are of concern, etc.) and type of operation (batch or continuous). The Venturi feeder is the most straightforward low-pressure feeding system. It consists of an air-entraining nozzle, where the high air velocity through the nozzle creates a region of negative pressure in which the material is entrained. It is suitable for relatively low particle concentration values. Medium-pressure systems are used where particles are prone to clump together. This system usually has a screw or pump system to supply the solid particles. High-pressure systems are used for conveying particles for long distances with very high values of particle-to-gas volume ratio [32].

Coupled with the feeding systems, the dispensing strategy allows the obtainment of the proper air flow contamination. In [31], methods to meter and disperse solid particles are shown. Such systems employ the capability of pressurized air, vibration, and volumetric devices to sample the solid contaminants with the proper repeatability over time. All systems are characterized by using a repetitive action to dose and deliver a precise volume of solid particles. The variation of the volume or the velocity of such sample operation determines the capability of the system to adjust the contamination of the airflow [31].

1.2. Aim of the work and novelty

This work aims to set up a straightforward methodology for calibrating an aerosol dosing and injection device. Micro-sized solid particles introduce several issues concerning their preparation, injection, and measurement. The description of the standard layout, the measurement procedure, and the data post-process are reported. The test facility, conceptualized to measure the contamination dose and the particle dispersion, is described in detail, together with the test procedure adopted for the calibration. The proper particle and fluid mixing process is also carefully checked and reported. Finally, the results related to the calibration curves obtained for the different powders are shown and compared.

To increase the usefulness of the present analysis, the experimental tests have been carried out using powders with different chemical compositions, physical properties, and size distributions. Moreover, the error source due to the sampling operation has been estimated and corrected. A method based on the particle Stokes numbers has been applied to correct the measured particle concentration, generating a valuable and straightforward process for several cases. The particle polydispersity is a crucial parameter in the present correction methodology. This work shows how similar multiphase tests are characterized by different correlations due to the other characteristics of the powder. The particle size and the diameter distribution represent the critical parameters for properly correcting the concentration values in multiphase flow measurements. According to the proposed correction procedure, a step forward in the controlling strategy of the feeder, as well as the reduction of the test uncertainty, can be carried out.

2. Test bench layout

The calibrating facility is located in the Fluid Machinery laboratory of the Engineering Department of the University of Ferrara (Italy). The circuit layout is reported in Fig. 1. The air enters through the filter section to ensure the removal of airborne particles. The filter used for this scope is a compact EPA F9 filter with dimensions 400 × 400 × 600 mm. The filter is located in a squared section frame that allows the connection of the filter to the primary circuit. The airflow is measured by a hot-wire mass flow meter, the TMASS 65, provided by Endress + Hauser, whose measurement range is between 20 and 2000 kg/h and its uncertainty is ± 1.5 % of the measured value. The installation procedure of the mass flow meter considers the presence of the upstream and

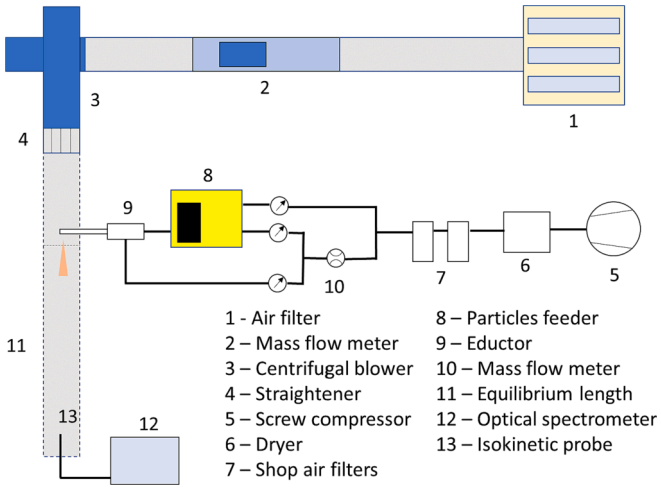

Fig. 1. Schematic view of the calibration test rig with all the components

downstream lengths to ensure an optimal operation of the device, avoiding the uncertainty source of the device installation. Upstream and downstream distances of 500 mm (equal to five equivalent hydraulic diameters) and 400 mm (equal to four equivalent hydraulic diameters), respectively, have been ensured. The air is blown through the circuit by a centrifugal blower. The outlet duct of the blower has a diameter of 150 mm. A straightener, mounted at the blower outlet and realized according to the standard UNI EN ISO 5802:2015, reduces the turbulence of the flow. Finally, the contaminated airflow is collected at the outlet by an exhausting system, avoiding the particle re-entrainment.

2.1. Dust injection system

The feeding system is designed to inject a constant amount of contaminant. A screw compressor supplies the air required to drive the system. A heat exchanger, located downstream of the compressor, removes moisture from the shop air, and a set of filters removes the impurities, such as dust and oil droplets. The clean and dry shop air follows three paths: two enter the particle feeder, and one goes to an aerodynamic eductor. The pressure on each line is adjusted using a pressure regulator. The air mass flow rate is measured by a thermal mass flow meter, the PFM750 model provided by SMC, whose uncertainty is ± 2 l/min.

The particle feeder is the SAG 410 Ultra-low Flow model made by TOPAS gmbh. This device provides the correct dosage of the powder mass constantly. The operating principle of the feeding system is shown in Fig. 2. As reported in [31], this type of dosing system ensures high instantaneous precision of the metering process and, at the same, it is suitable for continuous feeding process. A rotating ring is charged with the powder in a drizzling manner employing a conveyor system, and the powder, which forms a sort of layer on the upper ring surface, is carried at a constant speed from the charging site to the sucking dispersing nozzle. This dispersing nozzle, which equips the particle feeder, allows the first deagglomeration and dispersion of the powder. After the sucking zone, to ensure the repeatability of the dosing process, the ring is continuously cleaned by a brush that removes the residual (if present) particles on the rotating ring. Therefore, the ring surface is ready for a new charging cycle. The powder path from the reservoir to the charging zone on the ring is represented by a dashed line in Fig. 2. The picture of the dosing system during its operation is reported in Fig. 3. From this view, the charging site, with the flowing powder, and the powder carried on the ring are visible. In the right part of the charging site, a portion of the device can be noted where bigger agglomerates fall after bouncing the ring. Due to the design of this dosing system, agglomerates could drop onto the particle layer just deposited on the rotating ring. All the areas in which the behavior of particles is unpredictable make the calibration process the only viable and accurate way of having concentration curves that reliably represent the operating point of the feeder, ensuring that the multiphase flow measurement is realized with the proper contaminant dispersion and concentration.

The aerosol generator could be equipped with two rotating rings of different thicknesses: 0.3 mm and 1.0 mm. This leads to achieving a wide range of particle mass flow rates. The rotating speed of the dosing ring can be freely selected through a linear rheostat in terms of the percentage of the maximum speed. As reported in the following section, the modification of the ring rotating speed determines the modification of the injected mass flow rate. One of the paths of the supplied air is used to drive the dispersing nozzle, and the other one provides the purge air to maintain the feeder closure clean. The purge air prevents particles from saturating/being dispersed into the feeding chamber. This purging system avoids the particle re-entrainment process that could modify the amount of dosed particles. The dispersing nozzle operates in the feeder closure, and if it is not purged correctly, the presence of suspended particles increases the amount of dosed particles, introducing several meter inaccuracies. The third line of the supplied shop air drives the aerodynamic eductor. The eductor sucks and disperses the dust previously dosed by the feeder into the main duct. The aerodynamic eductor achieves the deagglomeration of the powder thanks to the shear stress applied by the Venturi nozzle [33,34].

Moreover, the aerodynamic eductor (i) provides the injection in

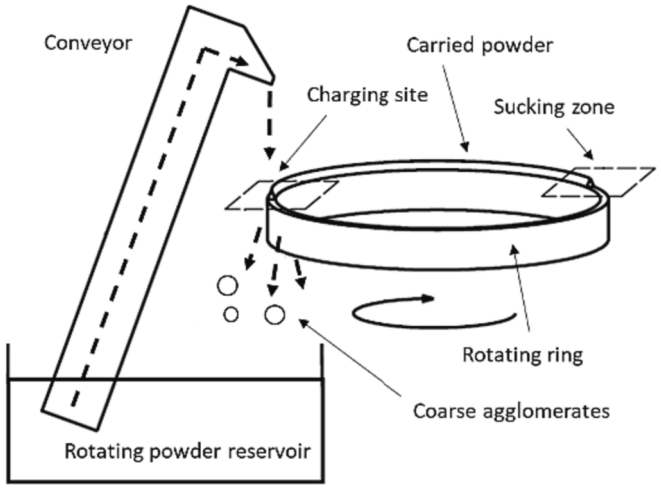

Fig. 2. Schematic view of the feeding operation

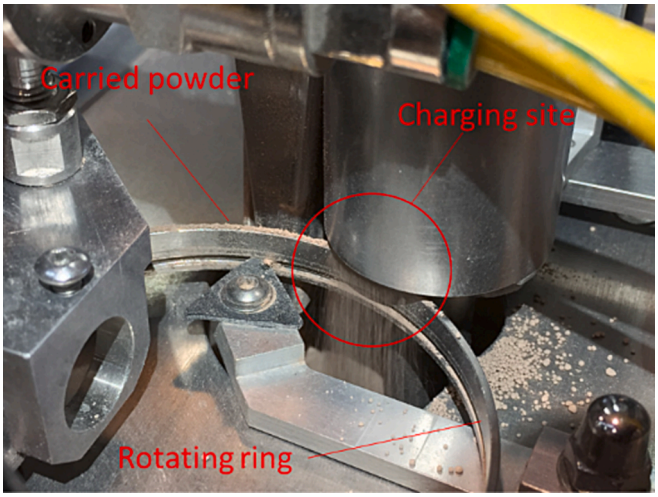

Fig. 3. Dosing section of the SAG 410 Ultra-low Flow

pressurized ducts since the feeder can not work with high back pressure, and (ii) injects the powders in the same flow direction. These two features allow the installation of the feeding system on several test benches operating in a wide range of pressure conditions. Therefore, the injection setup is based on the action of a Venturi disperser that avoids the injection of agglomerates and the influence of the back pressure.

Downstream the injection point, the sampling point has been placed at a distance equal to 2 m. This distance, called equilibrium length, allows the full coupling of the particles with the main airflow. The equilibrium length has been chosen by means of an iterative procedure based on the drag force acting on the particles. The expression of the drag force on a spherical particle is:

$$F_D = \frac{c_D Re_P \rho_{air} d_P^2 \pi (U - U_P)}{8} \quad (1)$$

where ρ_{air} is the fluid density, d_P is the particle diameter, U is the fluid velocity, U_P is the particle velocity, and c_D is the drag coefficient, a function of the Reynolds number of the particle:

$$Re_P = \frac{d_P (U - U_P) \rho_{air}}{\mu_{air}} \quad (2)$$

where μ_{air} is the fluid viscosity. In [35], the drag coefficient values are reported according to the Re_p ranges. Due to the polydispersity of the test dust, the calculation is provided with the conservative hypothesis of d_p equal d_{90} (see next section for more details about particle distribution). The iterative procedure calculates the distance traveled by the particle until the drag force reaches a value near zero, which means that the particle velocity is the same as the airflow velocity. The results have shown that an equilibrium length of 2 m is adequate for fully coupling the particles with the airflow. The achievement of the thermal equilibrium has been neglected in the present investigation.

2.2. Particle counting system

The online dust concentration measurement is provided at the downstream section of the equilibrium tube. The measurement is realized using the Particle Spectrometer OPS 3330 provided by TSI, representing the primary standard used in the present analysis. The physical principle behind this measurement technique is light scattering. The internal pump of the spectrometer sucks a portion of the contaminated air and goes through a laser beam. The internal vacuum pump is designed to suck a constant air flow rate of 1 l/min. The scattered light of the dust particles is collected by a mirror and measured by a photodetector that converts the information into the value of the particles counted. This measurement is provided continuously and gives the local particle concentration. The measurement range of the particle mass concentration is between 0.001 and 275000 μg/m^3. According to the calibration reports, the accuracy of the particle spectrometer used in the present analysis is estimated equal to ± 7 % in relation to the counting efficiency and 2.5 % in terms of particle sizing according to the standard ASHRAE 52.2-2017.

It is reasonable to assume that the local measure of the particle concentration is representative of the outlet concentration. This assumption is based on the fact that the sampling probe is placed in the undisturbed flow area (as far as possible from the walls to reduce the boundary layer effects), and the small cross-sectional area of the probe makes the potential impact negligible compared to the particle relaxation time. In addition, an isokinetic probe has been added to the sampling system to achieve the isokinetic sampling of the spectrometer. The suction duct of the probe is made of stainless steel and has a diameter of 1.25 mm, whereas the carrying body is made of copper.

This device guarantees the equality between the velocity at the inlet of the probe and the velocity of the undisturbed flow. This technique of sampling is crucial for concentration measurements. If the isokinetic condition is not respected, the under/over estimation of the concentration will be unavoidable [36,37]. In Fig. 4, schemes of the isokinetic and non-isokinetic sampling are shown. The basic principle is that the sample probe does not affect the flow field in its proximity, as reported in Fig. 4a. In this condition, smaller and bigger particles are not disturbed by the presence of the probe, and the local particle dispersion remains the same inside the probe tube. If U_0 is the velocity of the undisturbed flow and U is the velocity of the flow inside the probe, the underestimation of the particle concentration is due to a value of U/U_0 greater than one (Fig. 4b). In this condition, particles with great inertia (bigger particles) continue their path, and they are not captured by the probe, although only small particles follow the flow into the probe. Local airflow acceleration determines a lower particle count due to lower capability related to the catching process of bigger particles [37]. On the other hand, a value of the velocity ratio less than one leads to an overestimation of the particle concentration (Fig. 4c). In these conditions, coarse particles enter the probe, while small particles follow the streamlines that draw a stagnation effect due to the lower value assumed by the sampling velocity U [37]. Local stagnation determines a greater count for bigger particles instead of smaller ones. Therefore, a finer particulate sample is obtained where the sampling velocity is too high and a coarser particulate sample when the velocity is too low.

3. Methods and measurements

3.1. Powder characteristics

The micrometric powders selected for this work are Arizona Road Dust (ARD), alumina (Al_2O_3), and silicon carbide (SiC). The ARD is a silica-based standard powder for filter testing, and it is also widely used in experimental campaigns [16 –18,20,21,23,38,39]. Alumina and silicon carbide particles are also commonly used for aerosol testing [40 –44]. Two grades of ARD have been tested in this work: the Nominal (0 – 3) μm (ARD N) and ISO 12103-1 Ultra-Fine (ARD UF) [45], provided by Powder Technology Inc. The manufacturer provided the chemical

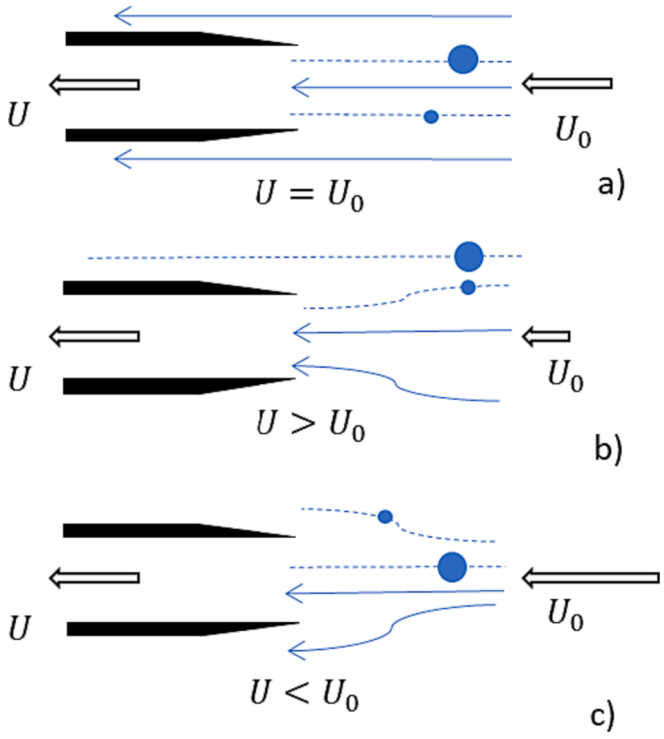

Fig. 4. Scheme of sampling conditions according to the particle inertia effects: a) isokinetic, b) non-isokinetic with the velocity inside the probe higher than undisturbed flow, and c) non-isokinetic with the velocity inside the probe lower than undisturbed flow. Figure freely inspired by [37]

properties and the diameter distribution of the two grades of ARD. The vendor did not offer Al_2O_3 and SiC properties, which were measured with in-house equipment. The powder diameter distribution is obtained using a sedigraph. The overall average density of the powder was determined by an AccuPyc II 1340 pycnometer. The particle density and the chemical composition of the materials are reported in Table 2. The diameter distributions of the powders are reported in Fig. 5. In Table 1, the values of d_{mean}, d_{10}, d_{50}, and d_{90} are reported. In Fig. 6, Scanning Electron Microscope (SEM) pictures are reported for each powder sample. The powder samples show, in all cases, the irregular shape of the grains coupled with the polydespersion of the particle dimension.

3.2. Powder preparation

Before starting the calibration procedure, the powders were prepared. The powder preparation ensures the total removal of the moisture absorbed by the environment. The presence of water inside the powder can affect the dosing process, providing a non-repeatable dosing operation and the mass deviation during the particle counts operation. High hydrophilic powders, such as Arizona Road Dust, are more prone to form agglomerates that can clog the injector, increasing the adhesion capabilities of the particles. If this condition occurs, the dosing operation is not repeatable and is strongly dependent on the humidity level of the environment [31]. The repeatability meter process is based on the power characteristics. Using a rotating disperser, agglomerates could change the loading process, and with the same rotating speed, the contaminant load changes. The preparation is done by baking the powders to ensure moisture removal. To assess the water content of each powder, the following procedure has been realized. A sample of the test powder, of approximately 3 g, was baked in an oven at 100 °C ± 2 °C for one hour. At the end of this operation, the sample weight is compared with its initial weight. The samples have been weighted using the analytic scale Kern ABT 100-5NM, with a resolution of 0,01 mg and a reproducibility value of ± 0,05 mg. The procedure was repeated until the weight was constant, as shown in the asymptotic value in Fig. 7. In Fig. 7, the weight loss trends during the backing procedure are reported. The ARD N has a high water content in percentage of the weight, around 5 %. The ARD UF has less than 1 % of water content. Instead, the alumina and silicon carbide powders have a minimum moisture content. These powder samples are more stable and independent with respect to environmental conditions due to their nature and chemical composition.

3.3. Airflow parameters

The choice of the airflow rate for the calibration is strictly related to the technical specifics of the sampling device. An optimal dilution of the aerosol into the airflow stream (i.e., the proper control of the contaminant concentration) ensures the overtime stability of the multiphase measurement process. Greater contaminant concentration could generate several agglomerates within the equilibrium lengths due to the excessive particle-to-particle interactions. At the same time, lower particle concentration could determine the impossibility of making relevant statistics with the sampling probe. Coupled with these multiphase peculiarities, properly selecting the contaminant concentration ensures the sampling device works in an optimal measurement range without reaching the full-scale value during the calibration operations. However, the more the airflow rate increases, the more the probe suction diameter must be reduced to ensure the isokinetic condition. Reducing the suction probe diameter requires a higher head of the device internal pump to maintain the flow rate constant (operating constraint of the device). This condition can overheat the internal parts and bring the device to failure.

Furthermore, when a higher aerosol concentration is tested, small-diameter-sampling probes are more prone to clog. For these reasons, a trial and error process in changing both probe diameter and air mass flow rate was necessary to define the suitable condition to calibrate the system for its entire range with all the tested powders. As a result, a probe with a diameter of 1.25 mm and an air mass flow rate of 1006 kg/h in the main circuit has been chosen. These parameters ensure the optimal operation of the sampling device and the achievement of the isokinetic condition.

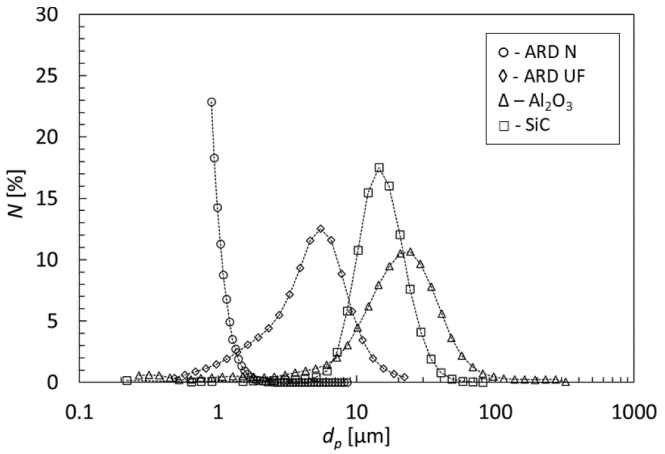

Fig. 5. Diameter distribution of the tested materials

Table 1
Test powders diameter distributions

Powder	d_{mean} [µm]	d_{10} [µm]	d_{50} [µm]	d_{90} [µm]
ARD N	1.3	0.9	1.1	1.9
ARD UF	4.8	1.1	4.3	8.5
Al_2O_3	25.2	5.7	20.1	43.9
SiC	16.0	8.8	14.7	24.8

Table 2
Density and chemical composition of the test powder materials

	ARD	Al_2O_3	SiC
ρ [kg/m^3]	2717	3870	3215
SiO_2	69.9	–	–
SiC	–	–	100
Al_2O_3	14.4	100	–
Na_2O	3.5	–	–
Fe_2O_3	4.7	–	–
CaO	2.6	–	–
MgO	1.9	–	–
K_2O	2.1	–	–
TiO_2	0.8	–	–

3.4. Calibration procedure

The same calibration procedure has been carried out for all the powders. Before starting the calibration, the system is cleaned. After the cleaning operations, the blower was turned on, and the operative mass flow rate value was achieved. The particle feeder reservoir is filled with powder, and the purge air is supplied to the feeder. The pressure of the purge air is kept at 4 bar. After this procedure, the main airline of the eductor is opened. This allows the air (without particles) to flow into the main duct. The eductor operating pressure is kept to 1 bar. Before starting the particle injection, the value of the particle concentration of the flowing air was recorded and used as an offset for the calibration. During this operation, it can be assessed that the particles do not flow from the feeder toward the main duct before the ring rotates. However, due to the presence of the filtration system, this value was very low, less than 10 particles/cm^3. The initial offset accounts for the filter media operation and the residual suspended particles that could be stuck in the injection systems and test bench-wetted internal surface after cleaning.

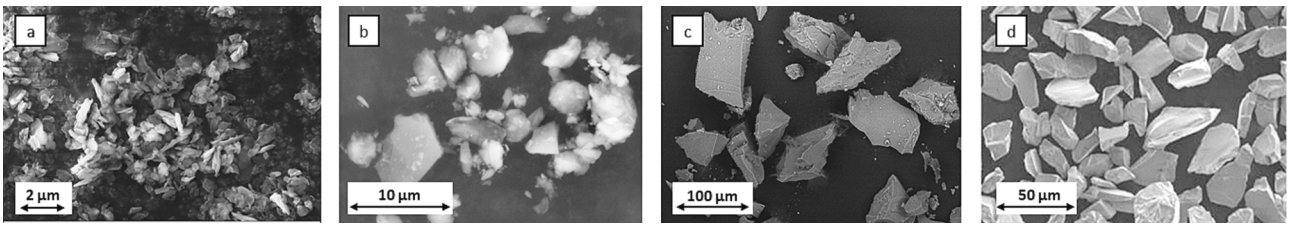

Fig. 6. SEM pictures of the powder samples: a) ARD N, b) ARD UF, c) Al2O3, and d) SiC

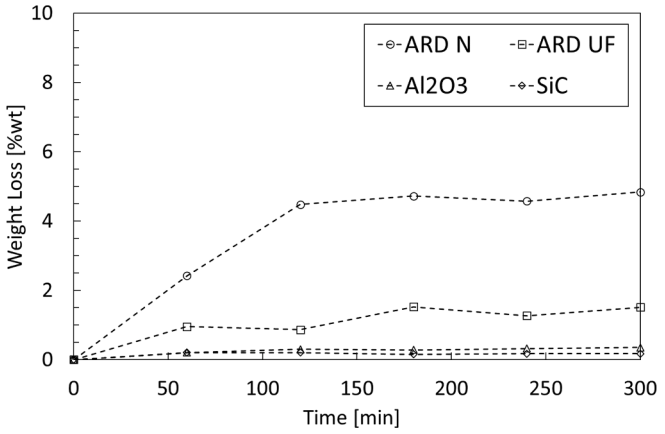

Fig. 7. Weight loss of the powder samples during the backing process

During the calibration operation, seven rotating speeds (RS) of the ring were tested, corresponding to 5 %, 10 %, 20 %, 40 %, 60 %, 80 %, and 100 % of the maximum value. Once the injection starts, the particle concentration is recorded for 160 s: every 10 s, the average particle concentration is acquired, obtaining 16 acquisitions for every RS. The calibration has been carried out with two dosing ring sizes (0.3 mm and 1.0 mm) for each powder. The combination of ring speed and thickness allows the variation of the particle concentration in a wide range, covering several applications from filter testing to erosive mechanism analysis. The calibration was repeated twice for each powder, evaluating the variation between the two independent calibration processes to ensure the repeatability of the procedure.

4. Sampling error estimation and correction

During the calibration procedures, the isokinetic condition was respected. As stated in paragraph 2.2 *Particle Counting System*, the isokinetic condition is reached when the air velocity into the main duct is equal to the air velocity into the sampling probe. This condition avoids the under or the overestimation of the particle concentration. However, despite the achievement of the isokinetic condition, the polydispersity of the aerosols tested can introduce sampling errors. This section explains the estimation of this sampling error and the correction method applied in this work. This calculation strategy completes the assessment of a precise and controlled contamination process of the airflow stream to generate reliable multiphase flow experiments. According to Belyaev and Levin [3], the relation used to correct the non-isokinetic sampling is expressed in the fashion of

$$\frac{C}{C_0} = 1 + \left(\frac{U_0}{U} - 1\right)\left(1 - \frac{1}{1 + (2 + 0.62U/U_0)Stk}\right) \tag{3}$$

where C is the concentration of the particles in the flow, C_0 is the real concentration, Stk is the Stokes number, U_0 is the velocity of the undisturbed flow, and U is the velocity in the sampling probe. When the ratio C/C_0 is near one, the isokinetic condition is respected, and the measured concentration corresponds to the actual concentration in the flow. As reported in Eq. 3, the ratio C/C_0 depends on the Stokes number of the particle, which is defined as:

$$Stk = \frac{d_P^2 U \rho_P}{18 L \mu_{air}} \tag{4}$$

where ρ_p is the particle density, d_p is the particle diameter, μ_{air} is the air viscosity, and L is the diameter of the sampling probe.

State this, the particle diameter distribution becomes critical to assess the correct value of the contaminant concentration. In the case of polydisperse aerosols, a distribution of Stk is obtained according to the particle diameter distribution (see Fig. 5 for reference). In this case, one value of the ratio C/C_0 for each diameter d_p can be calculated. Although the isokinetic condition can be corrected by Eq. 3, an error in the sampling process may occur. This error is more significant as the particle diameter increases, and the correction is based on the diameter distribution of the polydispersed powder sample. The correction value for the concentration of a single particle bin is obtained by dividing the percentage number of particles in the beam by the value of C/C_0 calculated with the beam diameter. Starting from the measured particle concentration $\overline{C}$, the actual particle concentration can be obtained:

$$\widehat{C}_0 = \overline{C} \sum_{i=1}^{k} \frac{\%N_i}{(C/C_0)_i} \tag{5}$$

where $\widehat{C}_0$ is the real particle concentration in the air stream, %N is the percentage of particle number, i indicates the diameter beam index, and k is the total number of beams of the particle number distribution. In Table 3, the values of the correction coefficient used in Eq. 5 are reported for the four different powders tested. The correction factor tends to one for the finest test powder, the ARD N. In these conditions, the measured concentration is near the real value, and the sampling error is low. In other cases, such Al_2O_3, a sampling error of up to 84 % may occur. The Al_2O_3 test dust, due to its coarse size and high density, is the powder most affected by the sampling error. The Fig. 8 summarizes the error estimation and correction procedure using a flow chart of data and formulas. The error can be reported in terms of mass by means of the powder distribution. Indicating with $d_{p,i}$ the particle diameter of the i-th particle beam and with N_i the percentage of the particles number in the beam, the mass error related to the sampling of a particle beam is:

$$e_i = \frac{N_i M_{p,i}(C/C_0 - 1)}{\sum_{i=1}^{k} N_i M_{p,i}} [\%] \tag{5}$$

where $M_{p;i}$ is the mass of a particle with diameter $d_{p,i}$ and k is the total number of beams. This value represents the error that affects a single beam if Eq. 3 is not used to correct the measurements. In Fig. 9, the mass error values of the powder samples tested are reported. As expected, the mass error is lower for the ARD N, with an average of 0.59 % of the total

Table 3
Values of the correction coefficient of the sampling error

	ARD N	ARD UF	Al_2O_3	SiC
$\sum_{i=1}^{k} N_i m_{p,i}$	0.83	0.59	0.16	0.49

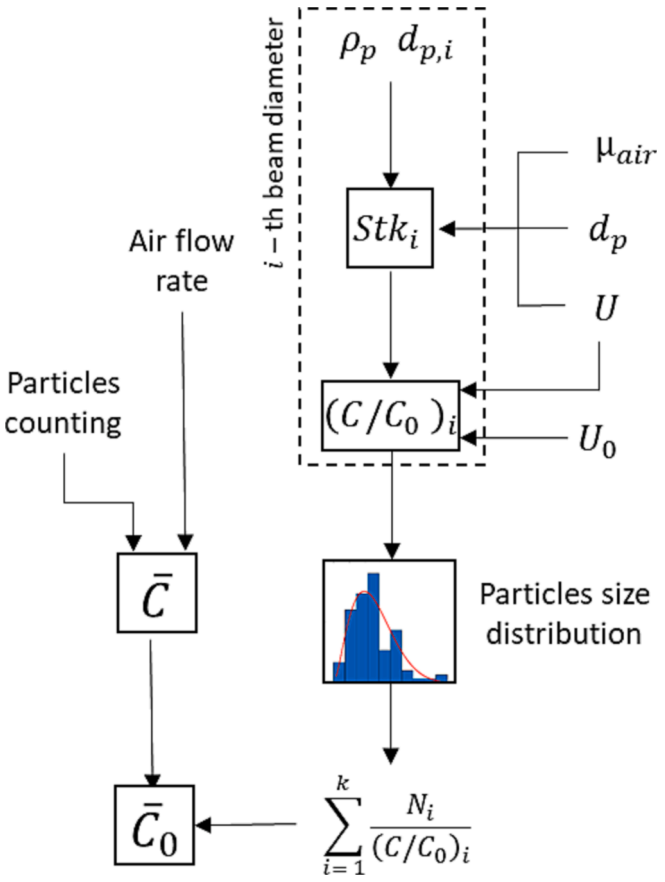

Fig. 8. Flow chart of the procedure applied to estimate and correct the sampling error

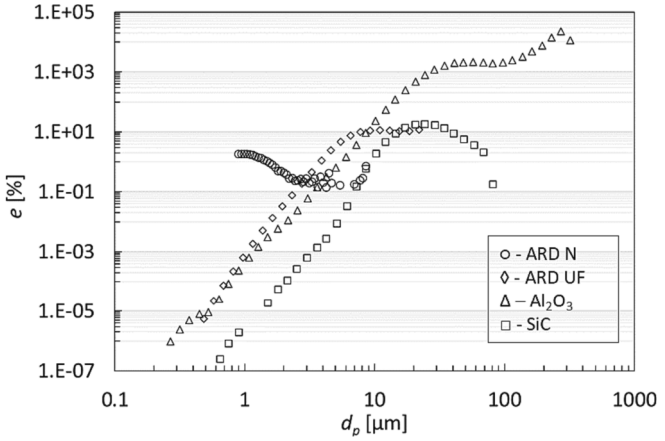

Fig. 9. Expected mass error as a function of the powder diameters if the correction is not applied

mass. The error increases to an average of 4.0 % and 4.2 % of the total mass for ARD UF and SiC, respectively. The Al_2O_3 reaches a higher average error that can lead to a tremendous overestimation of the mass injected. It can be concluded that the correction for the isokinetic flow condition proposed in Eq. 3 is not exhaustive when the powder sample is polydispersed, and specific test powders can give results affected by high errors. With the procedure reported in Fig. 8, the offline correction of these errors is mandatory if reliable measurements want to be achieved.

5. Calibration curves

The calibration curves are reported in Fig. 10 in terms of the powder mass flow rate injected. The curves have been reported as a function of the rotating speed of the ring. The rotating speed ring represents a reference to judging the dosing peculiarities. The variation of the speed ring is linear from 0 % to 100 %. As reported in [31], the operation of the rotating dispenser is based on the packing process of the powder and the uniformity of the powder sample.

The four charts report the curves obtained with the two rotating rings. The mass calculation is based on the diameter distribution reported in Fig. 5. For each rotating speed, the average value of the mass flow rate is shown with an error band indicating the standard deviation of the measurements. The standard deviation is calculated considering recorded samples (see paragraph 3.4 *Calibration Procedure*). As clearly visible in the graphs, the standard deviation is negligible for the measurement carried out in the case of the 1 mm-wide ring. This is mainly due to the stability and repeatability operation of a bigger ring. As described above, the ring is fed by a conveyor system, but agglomerated particles could fall and thus destroy the particle layer just deposited on the ring.

For this reason, a thicker ring allows the stability of the charging process, limiting the effects of agglomerates on the stability of the layer. However, the complexity of dosing the micro-sized particles implies the consideration of the random events that generate an instantaneous deviation from the smooth and standard operation of the feeder. Such a phenomenon has to be considered for longer experimental tests where the exposure time is greater than the characteristic time of such events. The repeatability performance of the ring, or, more in general, the dosing elements (ring, groove, or chamber), depends on the powder sample characteristics. Due to this, the feeder performance is strongly related to the particles, and therefore, a preliminary assessment has to be done before starting the experimental campaign.

The mass flow rate values are corrected following the procedure explained in section 4. *Sampling error estimation and correction* according to the flowchart proposed in Fig. 8. As shown in Fig. 10, the mass flow rate injected can vary by two orders of magnitude between the powders due to their different size and density. The calibration curves of Al_2O_3 and SiC (Fig. 10c and Fig. 10d) follow a straight line and appear stable as the rotating speed of the dosing ring increases. On the other hand, the ARD powders (Fig. 10a and Fig. 10b) have non-linear trends, especially when using the 1.0 mm dosing ring. The non-linear trend can be attributed to the combination of powder bulk properties and operating parameters of the dosing system device. The powder mass flow rate injected is related to the mass that remains on the ring surface when it leaves the charging zone. From the observation of the feeding operation (see Fig. 3), the more the rotating ring remains in the charging zone (low values of the RS), the faster the settled powder reaches its angle of repose (AoR). When the AoR is reached, the settled powder saturates the available ring surface, and, in these conditions, the mass flow rate injected depends only on the rotating speed of the ring. According to [46], the AoR is inversely proportional to the flowability of the powder. For example, alumina particles have a greater flowability and, thus, a lower AoR. The volumetric dosing system linearity is greater in the case of higher flowability. The charging site is based on the powder sample volume prepared by the feeder. The ring (or the groove) has a fixed geometry that represents the base of the stockpile. With a greater AoR and, thus, low flowability, the allowable stockpile height increases. When the ring speed is increased, the charging operation becomes faster, and only with a low AoR the charged volume on the ring remain the same, generating a linear trend between particle mass flow rate and ring speeds. By contrast, the variation of the loaded volume due to the greater available volume based on greater AoR and the ring speed variation determines non-linearity for sand particles. The charging time reduces as the rotating speed increases, and the ring saturation is even more challenging.

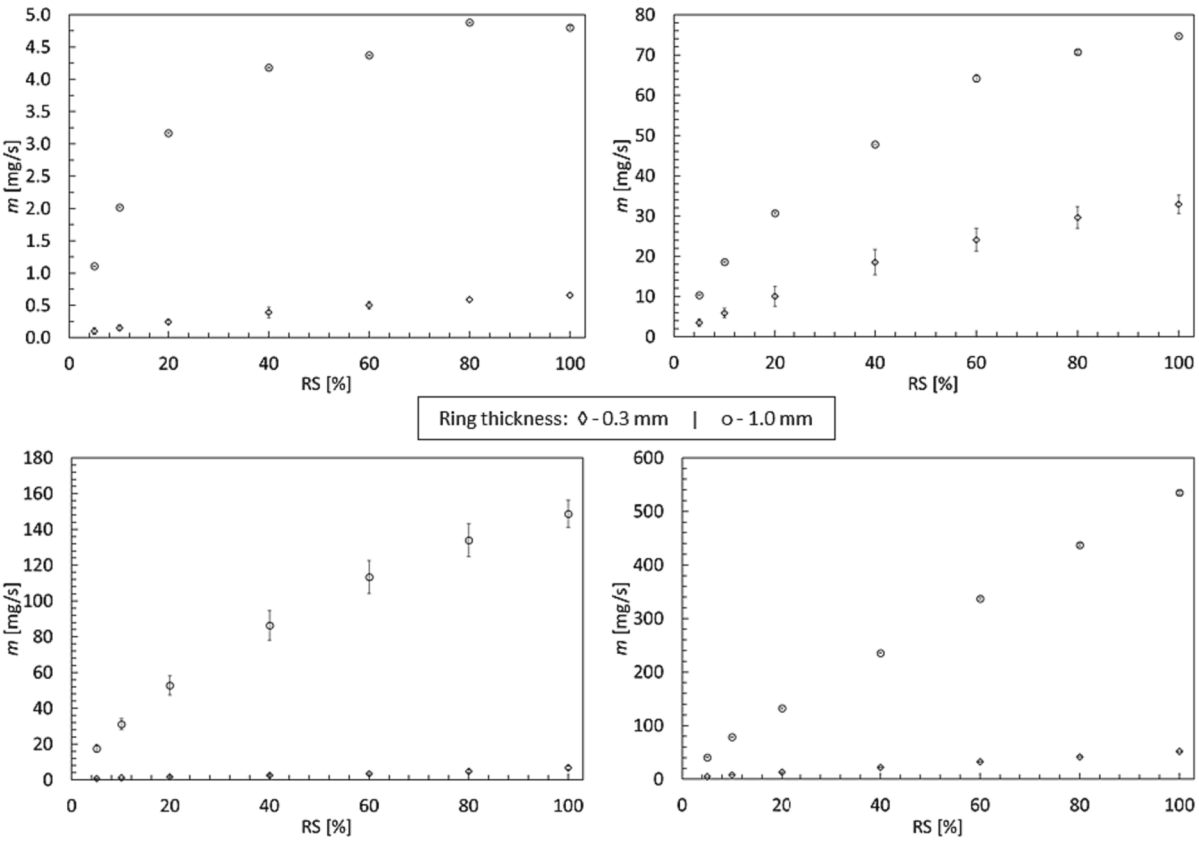

Fig. 10. Calibration curves of the feeding system as a function of the rotating speed of the dosing ring for a) ARD N, b) ARD UF, c) Al_2O_3, and d) SiC

The last analysis compares the mass flow rate provided by the two rings. Looking at Fig. 10, it is clear that the dosed mass flow rate is not proportional to the ring thickness for all the tested powder samples. According to the operating principle [31], by reducing the thickness of the ring (or the groove) by 3 times, the ideal dosed particle volume is reduced by 12.5 times if the ideal packing process is accounted. Fig. 11 compares the dosed mass for the two ring thicknesses for a given rotating speed ring. From the bar chart, ARD N and SiC powder samples show a constant ratio approximately equal to the nominal value (12.5) instead of Alumina and ARD UF, which offer a non-trivial trend. The ARD UF particles show a constant ratio equal to 3 over the whole range, while alumina particles show the most significant reduction characterized by an average value double than the ideal one. This analysis shows the cross-correlation between the powder bulk properties and the meter device. Different powder characteristics or particle diameter distributions for the same powder type could determine several non-linear effects. This non-linear effect is due to the AoR (responsible for the ring speed-related non-linearity) and the particle-to-particle and particle-to-ring interactions.

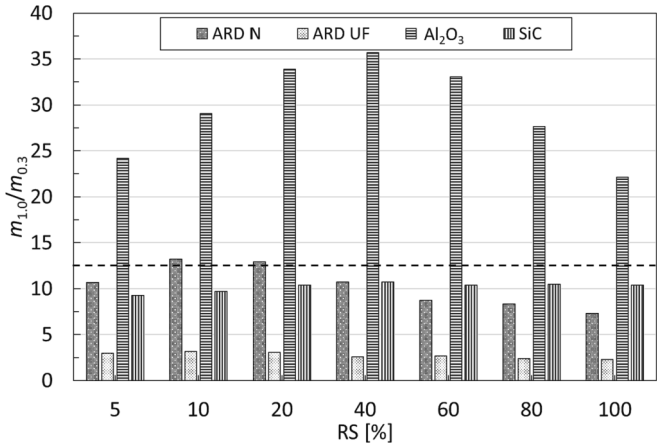

Fig. 11. Dosed mass ratio between the ring width of 1.0 mm and 0.3 mm

5.1. Guidelines

The present experimental analysis and the post-process methodology could represent a reference for the setup of multiphase flow experiments. The dosing system and the particle count process have to be designed and operated considering the effects of particle dynamics and airflow characteristics. Especially in the case of microsized particles, the proper control of airflow contamination can be developed by considering the following:

- the diameter distribution of the powder sample;
- the particle density concerning the gas media density and the gas-to-particle interaction represented by the Stokes number; the *iso*-kinetic condition is based on particle inertia, and the corrections are needed to control the metering process and/or measure the airflow contamination;
- the volumetric feeder repeatability and linearity depend on the powder bulk characteristics (e.g., angle of repose) and particle diameter distributions;
- the polydispersity of the powder sample coupled with the meter features implies the correction of the measure obtained by the particle counting system. A non-repeatable meter process could determine the modification of the a posteriori correction process of the particle concentration in the airflow.

In addition, the powder-related characteristics, such as the hygroscopicity and electrostatic action, determine that the multiphase

experiments must also be designed considering the preparation phase to increase the stability and repeatability of the measure. Proper overtime control of the metering and dispersion processes has to be provided to avoid deviations and drift during the contamination tests.

6. Conclusions

The calibration procedure of an aerosol dosing system for wind tunnel applications is described. The calibration apparatus has been explained in detail, and the operating parameters and the calibration procedure have been presented. Four powder samples have been selected to test and calibrate the feeding device using a particle spectrometer. The tested powders have been analyzed, and the physical and chemical properties, diameter distribution, and moisture content have been reported. The sampling error due to the polydispersity of the aerosol has been determined. It is found that, although the isokinetic condition during the calibration has been respected, sampling errors due to the polydispersity of the test dust may occur. The error estimation and correction methods have been applied to the calibration curves to remove the sampling error. Finally, the calibration curves obtained for the four test powders have been shown. The curves have been corrected, providing the method reported in the present work. The calibration curves show non-linear trends due to the combination of powder bulk properties, angle of repose, diameter distribution, and operating procedure of the dosing device. The non-linear effect appears evident for smaller particles (the two Arizona Road Dust tested), leading to a higher difficulty in handling and dosing processes. The methodology of the calibration process can be extended and generalized to other feeding systems and powder types. Peculiarities and features related to multiphase experimental analysis are reported for a wide range of micro-sized powders to increase the accuracy and test reliability.

Declaration of Competing Interest

The authors declare that they have no known competing financial interests or personal relationships that could have appeared to influence the work reported in this paper.

Data availability

Data will be made available on request.

References

[1] J.B. Barlow, W.H. Rae, A. Pope, Low-speed Wind Tunnel Testing, third ed., John Wiley & Sons Inc, 1999.
[2] N.A. Fuchs, Sampling of aerosols (1975), Atmos. Environ. 9 (8) (1967) 697–707.
[3] S.P. Belyaev, L.M. Levin, Techniques for collection of representative aerosol samples, J. Aerosol Sci. 5 (4) (1974) 325–338.
[4] D.K. Heist, J. Richmond-Bryant, A. Eisner, T. Conner, Development of a versatile aerosol generation system for use in a large wind tunnel, Aerosol Sci. Tech. 37 (3) (2003) 293–301.
[5] F.O. Arouca, N.R. Feitosa, J.R. Coury, Effect of sampling in the evaluation of particle size distribution in nanoaerosols, Powder Technol. 200 (1–2) (2010) 52–59.
[6] J. Wagner, D. Leith, Passive aerosol sampler. Part II: Wind tunnel experiments, Aerosol Sci. Technol. 34 (2) (2001) 193–201.
[7] O. Witschger, R. Wrobel, J.F. Fabriès, P. Görner, A. Renoux, A new experimental wind tunnel facility for aerosol sampling investigations, J. Aerosol Sci 28 (5) (1997) 833–851.
[8] R. Oliveira, Understanding adhesion: A means for preventing fouling, Exp. Therm Fluid Sci. 14 (4) (1997) 316–322, https://doi.org/10.1016/S0894-1777(96)00134-3.
[9] Y. Ichikawa, K. Shinoda, Current status and challenges for unified understanding of bonding mechanism in solid particle deposition process, Mater. Trans. 62 (6) (2021) 691–702, https://doi.org/10.2320/matertrans.T-M2021813.
[10] A. Chowdhury, H.G. Johnston, C.V. Mashuga, M.S. Mannan, E.L. Petersen, Effect of particle size and polydispersity on dust entrainment behind a moving shock wave, Exp. Therm Fluid Sci. 93 (2018) 1–10, https://doi.org/10.1016/j.expthermflusci.2017.12.002.
[11] R. Tarodiya, A. Levy, Surface erosion due to particle-surface interactions - A review, Powder Technol. 387 (2021) 527–559, https://doi.org/10.1016/j.powtec.2021.04.055.
[12] N. Miyazaki, Solid particle erosion of composite materials: A critical review, J. Compos. Mater. 50 (23) (2016) 3175–3217, https://doi.org/10.1177/0021998315617818.
[13] S.C.S. Costa, A.S.A.C. Diniz, L.L. Kazmerski, Solar energy dust and soiling R&D progress: Literature review update for 2016, Renew. Sustain. Energy Rev. 82 (2018) 2504–2536, https://doi.org/10.1016/j.rser.2017.09.015.
[14] M. Awais, A.A. Bhuiyan, Recent advancements in impedance of fouling resistance and particulate depositions in heat exchangers, Int. J. Heat Mass Transf. 141 (2019) 580–603, https://doi.org/10.1016/j.ijheatmasstransfer.2019.07.011.
[15] J. Visser, Particle adhesion and removal: a review, Part. Sci. Technol. 13 (1995) 169–196.
[16] A. Suman, M. Morini, N. Aldi, N. Casari, M. Pinelli, P.R. Spina, A compressor fouling review based on an historical survey of asme turbo expo papers, J. Turbomach. 139 (2017), 041005.
[17] A. Suman, A. Vulpio, N. Casari, M. Pinelli, Outstretching population growth theory towards surface contamination, Powder Technol. 394 (2021) 597–607.
[18] N. Casari, A. Fortini, M. Pinelli, A. Suman, A. Vulpio, N. Zanini, Measurement approaches for the analysis of soil layer by microparticle adhesion, Measurement: Journal of the International Measurement Confederation 187 (2022). art no. 110185. https://doi.org/10.1016/j.measurement.2021.110185.
[19] S.A. Lawson, K.A. Thole, Simulations of multiphase particle deposition on endwall film-cooling holes in transverse trenches, J. Turbomach. 134 (5) (2012), 051040.
[20] A. Suman, A. Vulpio, N. Casari, M. Pinelli, R. Kurz, K. Brun, Deposition pattern analysis on a fouled multistage test compressor, J. Eng. Gas Turbines Power 143 (8) (2021). art . no. 081006. https://doi.org/10.1115/1.4049510.
[21] A. Suman, N. Casari, E. Fabbri, L. di Mare, F. Montomoli, M. Pinelli, Generalization of particle impact behavior in gas turbine via non-dimensional grouping, Prog. Energy Combust. Sci. 74 (2019) 103–151.
[22] A. Suman, N. Casari, E. Fabbri, M. Pinelli, L. Di Mare, F. Montomoli, Gas turbine fouling tests: review, critical analysis, and particle impact behavior map, J. Eng. Gas Turbines Power 141 (3) (2019). art no. 032601. https://doi.org/10.1115/1.4041282.
[23] A. Vulpio, A. Suman, N. Casari, M. Pinelli, R. Kurz, K. Brun, Analysis of timewise compressor fouling phenomenon on a multistage test compressor: performance losses and particle adhesion, J. Eng. Gas Turbines Power 143 (8) (2021). art no. 081005. https://doi.org/10.1115/1.4049505.
[24] W. Tabakoff, T. Wakeman, Test facility for material erosion at high temperature, in: Erosion: Prevention and Useful Applications (1979), ASTM International, STP35798S pp. 123-135.
[25] A. Suman, N. Zanini, M. Pinelli, Design of an innovative experimental rig for the study of deposition phenomena in axial compressors, Proc. of the ASME Turbo Expo (2023). Paper Number GT2023-103408.
[26] D.Q. Kern, R.E. Seaton, Surface fouling: How to calculate limits, Chem. Eng. Prog. 55 (1959) 71–73.
[27] J.A. Stasiek, Experimental studies of heat transfer and fluid flow across corrugated-undulated heat exchanger surfaces, Int. J. Heat and Mass Transfer, 41 (6-7) (1998), pp. 899–914.
[28] H. Müller-Steinhagen, M.R. Malayeri, A.P. Watkinson, Recent advances in heat exchanger fouling research, mitigation, and cleaning techniques, Heat Transfer Eng. 28 (3) (2007) 173–176.
[29] I.H. Bell, E.A. Groll, H. König, Experimental analysis of the effects of particulate fouling on heat exchanger heat transfer and air-side pressure drop for a hybrid dry cooler, Heat Transfer Eng., 32 (3-4) (2011), pp. 264–271.
[30] Anuar F. Shikh, K. Hooman, M.R. Malayeri, Abdi I. Ashtiani, Experimental study of particulate fouling in partially filled channel with open-cell metal foam, Experim. Therm. Fluid Sci., 110 (2020), art. no. 109941, DOI: 10.1016/j.expthermflusci.2019.109941.
[31] S. Yang, J.R.G. Evans, Metering and dispensing of powder; the quest for new solid freeforming techniques, Powder Technol. 178 (1) (2007) 56–72, https://doi.org/10.1016/j.powtec.2007.04.004.
[32] G.E. Klinzing, F. Rizk, R. Marcus, L.S. Leung, Pneumatic Conveying of Solids: A theoretical and practical approach, third ed., Springer Dordrecht, Netherland, 2011. DOI: 10.1007/978-90-481-3609-4.
[33] Y. Endo, S. Hasebe, Y. Kousaka, Dispersion of aggregates of fine powder by acceleration in an air stream and its application to the evaluation of adhesion between particles, Powder Technol. 91 (1) (1997) 25–30.
[34] G. Calvert, M. Ghadiri, R. Tweedie, Aerodynamic dispersion of cohesive powders: A review of understanding and technology, Adv. Powder Technol. 20 (1) (2009) 4–16.
[35] R. Clift, J.R. Grace, M.E. Weber, Bubbles, Drops, and Particles, Dover Civil and Mechanical Engineering Series Dover books on engineering, Courier Corporation, 2005.
[36] W.C. Hinds, Y. Zhu, Aerosol technology: properties, behavior, and measurement of airborne particles, third ed., John Wiley & Sons Inc, 2022.
[37] J.D. Wilcox, Isokinetic flow and sampling, J. Air Pollut. Control Assoc. 5 (4) (1956) 226–245.
[38] A. Suman, A. Vulpio, N. Casari, M. Pinelli, F. di Lillo, L. D'Amico, Analysis of soil and soot deposits by X-ray computed microtomography, Powder Technol. 394 (2021) 608–621.
[39] A. Suman, A. Vulpio, M. Pinelli, L. D'Amico, Microtomography of soil and soot deposits: analysis of three-dimensional structures and surface morphology, J. Eng. Gas Turbines Power, 144 (10) (2022), art. no. 101010. https://doi.org/10.1115/1.4055217.

[40] D. Mark, J.H. Vincent, H. Gibson, W.A. Witherspoon, Applications of closely graded powders of fused alumina as test dusts for aerosol studies, J. Aerosol Sci 16 (2) (1985) 125–131.
[41] F.L. Crosswy, Particle size distributions of several commonly used seeding aerosols, NASA Conference Publication, 1985, pp. 53 - 75.
[42] M. Morgeneyer, O. Le Bihan, A. Ustache, O. Aguerre-Chariol, Experimental study of the aerosolization of fine alumina particles from bulk by a vortex shaker, Powder Technol. 246 (2013) 583–589.
[43] J. Exner, M. Hahn, M. Schubert, D. Hanft, P. Fuierer, R. Moos, Powder requirements for aerosol deposition of alumina films, Adv. Powder Technol. 26 (4) (2015) 1143–1151.
[44] T. Poppe, J. Blum, T. Henning, Analogous experiments on the stickiness of micron-sized preplanetary dust, Astrophys. J. 533 (1 PART 1) (2000) 454–471.
[45] ISO 12103-1:2016. Road vehicles - Test contaminants for filter evaluation - Part 1: Arizona test dust.
[46] H.M. Beakawi Al-Hashemi, O.S. Baghabra Al-Amoudi, A review on the angle of repose of granular materials, Powder Technol. 330 (2018) 397–417, https://doi.org/10.1016/j.powtec.2018.02.003.